Greenland Ice Sheet late-season melt: Investigating multi-scale drivers of K-transect events

Thomas J. Ballinger, Thomas L. Mote, Kyle Mattingly, Angela C. Bliss, Edward Hanna, Dirk van As, Melissa Prieto, Saeideh Gharehchahi, Xavier Fettweis, Brice Noël, Paul C.J.P. Smeets, Carleen H. Reijmer, Mads H. Ribergaard, and John Cappelen

Manuscript submitted on 19 December 2018, revised on 10 April 2019 & 15 July 2019

Editor's Comments

Your revised manuscript was sent for another round of reviews (to the same referees who reviewed your first draft) as the referees suggested major revisions. I've now heard back from two of the referees (see the referee's comments below). Based on these comments, mainly from the reviewer #1, I ask you to carefully revise your manuscript before I can consider it for publication. Please note that TC journal cares about the conventional structure of scientific papers and authors are discouraged from moving the bulk of key figures to the supplementary material, as well as from referencing the *whole* methodology to previously published papers. I encourage you to add more substance and to improve the clarity of material presented in the Methods section, despite this resulting in additional few pages to your manuscript.

Authors' Statement

We thank the editor and reviewers (whose comments are addressed below) for the thoughtful and constructive comments on our revised manuscript. We have considered and subsequently addressed concerns and we believe revisions made on the current version have strengthened the paper, and hope improvements have now rendered the manuscript suitable for publication.

To summarize, the editor's main concerns were that key figures to the manuscript's story needed to be integrated into the manuscript and the methodology needed to more explicit and detailed in describing the techniques utilized in the study. In response to the concern over key figure placement, we have integrated the majority of the figures into the main text of the paper to smooth the reading process. In response to the methodological concern, we have expanded our description of both the integrated vapor transport (IVT) metric and the self-organizing map classification of IVT (please see Section 3, i.e. Methods)

The series of minor revisions by Anonymous Referee #2 have also been addressed. In carefully considering and addressing these areas, we believe the manuscript is greatly improved from the first revision. In the responses that follow, reviewer comments are shown in *italics* while author responses are provided in the red color used here.

Report #1/Anonymous Referee #2

Review of the revised manuscript of Ballinger et al., The Cryosphere Discussions, April 2019

In view of the online discussion, the manuscript maintains an unorthodox structure. There are good reasons why there are strict boundaries among different sections in scientific writing, and I am sure the experienced authoring team agrees. The Results section is still largely based on supplementary material, which is at the very least inconsiderate toward the reader. These aspects remain serious disadvantages of a study that begins sprinting and purposely trips itself.

As far as the science is concerned, the manuscript appears improved. Apparent mistakes and wrong statements previously evident in the manuscript have been corrected. The study now adopts moderate language appropriate for statistical analyses.

We appreciate the reviewer re-reviewing our paper. To improve flow and readability, we have integrated most of the supplemental material into the body of the revised manuscript.

Specific comments:

L115-117: There is logical inconsistency in this justification: KAN_B plays a central role in the study, so perhaps describe what is so special about KAN_B, why it is considered as reference, and then explain how its operational timespan limits the study period. Also, is KAN_B actually uninfluenced by flow patterns through the local topography?..

We have clarified the importance of KAN_B in Section 2.2, indicating that its location is nearest the ocean (relative to the other K-transect AWS sites) and proximate location to the terminus makes it a logical location from which to composite air temperatures. We also mention that inclusion of KAN_B allows us to maximize the longitudinal (west-to-east) extent from which to assess possible maritime influences on K-transect temperature conditions.

Regarding the large-scale atmospheric circulation, while the near-surface KAN_B winds are weaker relative to the higher elevation K-transect AWS sites (Fig 2b), the MAR and RACMO winds suggest the low-level flow, influenced by synoptic and katabatic regimes, is roughly consistent from KAN_B to KAN_M (see T+ composite maps in **Fig 7** and **Fig 8** in the revised manuscript). Further assessments of large-scale circulation attribution to T+ and T- events are left for future work.

L124: How can there be "erroneously low" daily temperature and wind averages? Are there also erroneously high daily averages?

We have removed reference to erroneous extremes as these were unintentionally leftover from humidity analyses removed from the manuscript. The sentence has been clarified to reflect that missing values were removed, and not estimated, before analyses were undertaken.

L160: Specify that it is above-freezing daily Tair. At the end of the sentence, cite a suitable, positive degree-day modeling study and/or Hock (2005).

We have added the Hock (2005) citation as recommended.

L165-166: Is sea-ice positively correlated with Tair?

We have restructured the sentence to more clearly reflect the correlations between Tair and sea ice freeze onset and SSTs noted in Hanna et al (2009) and Ballinger et al (2018).

L168-170: Unclear to me.

We have revised the sentence to more clearly express our composite methodology.

L199: End of the Northwest Atlantic melt season area: What is this in reference to? Very unclear.

We have changed the wording here to be more clear and specific, and have included the figure mentioned in the sentence. The sentence now reads " Time series depicting the conclusion of melt conditions across Baffin Bay and the western GrIS are shown in **Fig. 2**."

L199: Upward?..

We have removed "upward" and made the sentence more concise by beginning it with "Later sea ice formation…

L208: on average 6 days later

We have made the suggested change.

L217-220: This sentence is redundant, at least at this point.

We have removed this sentence.

L220: I am still missing why KAN_B is so special.

In the revised description of the K-transect AWS data (Section 2.2) that is motivated by the L115-117 comments previously addressed, we have clarified language justifying the use of KAN_B for analyses throughout the paper.

L225-227: I would begin with KAN_B, which receives stronger, more southerly winds during T+ events that tend to become weaker and more southerly in autumn. There is general wind-speed increase during T+ events, while direction remains more or less unaltered. Statistically significant directional change is always more southerly, which seems to be more evident above long-term ELA.

We have clarified this paragraph as follows: "KAN_B receives stronger, more southerly winds during T+ events that tend to become weaker and more southerly in autumn (i.e. [-30,-1]).

There tends to be a general wind speed increase during T+ events, while direction remains more or less unaltered. Statistically significant directional change is more southerly, which is evident above the long-term equilibrium line altitude at S9."

L232: Open water persistence is unclear to me.

We have changed the phrasing, which now reads "longer periods of nearshore open water."

L233: Define MSLP in the text.

We have spelled out the acronym.

L245: RMSE = … [units]

We have added the correct unit in reference to the wind speed (ms^{-1}).

L248: Why except? I don't see it.

We have removed "Except during [-30,-1] T+ events" and clarified references to the low-level wind composites presented in **Figs. 7 and 8**.

L263-264: It already becomes apparent from Fig. 5 that the furthest in autumn, the higher IVT is necessary for T+ events to occur. Good thing to mention here before analyzing the last figure.

This is a good point to highlight, and we have changed the sentence wording to reflect that higher IVT not only produces melt events, but greater vapor quantities are needed to produce melt as autumn progresses. This point is also now emphasized in the Abstract.

L270: Change enhance with cause?..

We have the suggested change.

L290: Fig. S7?..

We have corrected the figure number upon integrated most of the supplemental material. The referenced figure is now **Fig S1**.

L295: The word forcing is redundant.

We have removed "forcing" as recommended.

L298: Change manuscript with study.

We have made the suggested change.

Report #2/Anonymous Referee #3

Overall, I am happy with the revisions made. The authors acknowledge the inherent limitations of making temporal conclusions solely based upon a 5-year time period, but have adjusted the text to reflect that. With the short time period involved, it is (in my opinion) still difficult to make strong conclusions about temporal atmospheric changes, however the results are very suggestive and very worthy of further exploration (which the authors have expressed interest in pursuing). The hypotheses are presented in a way that encourages other groups to test or build upon them with other studies. I think this is a good contribution to the science, the concerns I had in the original manuscript have been addressed, and any particular critiques from me at this point could be categorized as "nitpicking." Thus, I recommend publishing the revised manuscript as is, assuming the other referees are as satisfied.

We appreciate the reviewer taking the time to review our revised paper.

Greenland Ice Sheet late-season melt: Investigating multi-scale drivers of K-transect events

Thomas J. Ballinger[1], Thomas L. Mote[2], Kyle Mattingly[2], Angela C. Bliss[3], Edward Hanna[4], Dirk van As[5], Melissa Prieto[1], Saeideh Gharehchahi[1], Xavier Fettweis[6], Brice Noël[7], Paul C.J.P. Smeets[7], Carleen H. Reijmer[7], Mads H. Ribergaard[8], and John Cappelen[8]

Correspondence to: Thomas J. Ballinger (tballinger@txstate.edu)

[1]Department of Geography, Texas State University, San Marcos, TX, USA
[2]Department of Geography, University of Georgia, Athens, GA, USA
[3]College of Earth, Ocean, and Atmospheric Sciences, Oregon State University, Corvallis, OR, USA
[4]School of Geography and Lincoln Centre for Water and Planetary Health, University of Lincoln, Lincoln, UK
[5]Geological Survey of Denmark and Greenland, Copenhagen, Denmark
[6]Laboratory of Climatology, Department of Geography, University of Liège, Liège, Belgium
[7]Institute for Marine and Atmospheric Research, Utrecht University, Utrecht, the Netherlands
[8]Danish Meteorological Institute, Copenhagen, Denmark

Manuscript submitted to *The Cryosphere Discussions* on 19 December 2018, revised on 10 April 2019 and 15 July 2019

Abstract. One consequence of recent Arctic warming is an increased occurrence and longer seasonality of above-freezing air temperature episodes. There is significant disagreement in the literature concerning potential physical connectivity between high-latitude open water duration proximate to the Greenland Ice Sheet (GrIS) and late-season (i.e. end-of-summer and autumn) GrIS melt events. Here, a new date of sea ice advance (DOA) product is used to determine the occurrence of Baffin Bay sea ice growth along Greenland's west coast for the 2011–2015 period. Over the two month period preceding the DOA, northwest Atlantic Ocean and atmospheric conditions are analyzed and linked to late-season melt events observed at a series of on-ice automatic weather stations (AWS) along the K-transect in southwestern Greenland. Surrounding ice sheet, tundra, and coastal winds from Modèle Atmosphérique Régional (MAR) and Regional Atmospheric Climate Model (RACMO) provide high-resolution spatial context to AWS observations, and are analyzed along with ERA-Interim reanalysis fields to understand the meso-to-synoptic scale (thermo)dynamic drivers of the melt events. Results suggest that late-season melt events, which primarily occur in the ablation area, are strongly affected by ridging atmospheric circulation patterns that transport warm, moist air from the sub-polar North Atlantic toward west Greenland. Increasing concentrations of North Atlantic water vapor are shown to be necessary to produce melt conditions as autumn progresses. While thermal conduction and advection off south Baffin Bay open waters impact coastal air temperatures, local marine air incursions are obstructed by barrier flows and persistent katabatic winds along the western GrIS margin.

Formatted: Not Highlight

Deleted: AWS wind speed and direction characteristics are evaluated for above and below-freezing surface-air temperature events before the DOA occurs.

Deleted: findings

Deleted: ring

Deleted: of the K-transect

Deleted: .

1 Introduction

Substantial decline in Arctic sea ice extent and mass loss from the Greenland Ice Sheet (GrIS) have been observed for the last four decades (e.g. Serreze and Stroeve, 2015; Bamber et al., 2018). Under sustained climate warming, sea and land ice are becoming increasingly sensitive to changes in the frequency and duration of anomalous weather patterns (e.g. Overland and Wang, 2016; Hanna et al. 2014, 2018b). The overall mass balance of the GrIS has contributed roughly 0.5 mm year^{-1} to global mean sea level rise since the early 1990s (van den Broeke et al., 2016), with about 60% of the mass loss attributed to a decline in surface mass balance (SMB) and 40% associated with increased ice discharge (van den Broeke et al., 2017). Observed warming of near-surface ocean waters west of Greenland since at least the early 1990s is linked to accelerated submarine melt and outlet glacier retreat (Holland et al., 2008; Straneo and Heimbach, 2013) concurrent with more frequent summertime air temperature extremes along the coast (Hanna et al., 2012, Mernild et al., 2014). These findings raise the question of whether Baffin local ocean conditions are of importance in governing the spatial extent and temporal variations in western GrIS melt.

Conflicting evidence has been presented in literature over the past decade regarding the importance of the warming of the nearby ocean on GrIS surface melt. Regional climate model simulations have suggested that local sea surface temperature (SST) impacts on GrIS climate and SMB are negligible due to offshore flow arising from a prevailing katabatic wind regime (Hanna et al., 2014; Noël et al., 2014). Using a statistical approach, Rennermalm et al. (2009) found contemporaneous Baffin open water (<15% sea ice concentration (SIC)) and western GrIS melt to be positively correlated in late summer (1979–2007). The authors noted that the strongest, statistically significant correlation (r=0.71) was observed in August near the K-transect (**Fig. 1**), and was attributed, in part, to wind-driven onshore transport of warm marine air. Hanna et al. (2009) evaluated lagged correlations between July coastal air temperatures at Ilulissat and Nuuk (~200 km north and ~300 km south of Kangerlussuaq, respectively) from Danish Meteorological Institute (DMI) weather stations and adjacent, offshore HadISST1 SST values in the preceding and following 2 months. The authors noted a simultaneous, positive SST relationship with Ilulissat temperatures (r=0.56), while Nuuk temperatures were significantly correlated with offshore May–July SSTs (r>0.50) over the 1977–2006 record. Ballinger et al. (2018a) found significant interannual correlations (r>0.40, p≤0.05) during 1979–2014 between Baffin freeze onset dates (from the Markus et al., 2009 product) and September–December surface air temperatures (SAT) at most DMI stations found along the west Greenland coastline. The authors found that significant, positive correlations between Baffin and Labrador SST and coastal SAT often persist through December after the onset of freeze. Applying a similar approach and melt/freeze dataset, Stroeve et al. (2017) showed Baffin and GrIS melt and freeze behaviors to be synchronous. The authors noted that years with anomalously early sea ice melt tended to have strong, upward turbulent heat fluxes and westerly winds atop developing open water that transported surplus heat and moisture onto the ice sheet. Both studies indicated that the synoptic, upper-level circulation pattern is critical for modulating poleward heat and moisture transport and the surface warming/melt processes toward the end of the melt season. Ballinger et al. (2018a) proposed a sea ice-heat flux feedback whereby upward turbulent heat fluxes from Baffin Bay help maintain the high-pressure block aloft, with anticyclonic southerly winds both inhibiting the autumn/winter ice pack formation and transporting warm marine air onto the western Greenland coast. This potential

mechanism may have contributed to record Greenland Blocking events that occurred in October over successive years during the early-to mid-2000s (Hanna et al., 2018a).

A paucity of literature focused on the Baffin Bay open water influence on GrIS melt and SMB has left open the question of potential physical linkages. Our primary goal in this paper is to evaluate and determine whether the local ocean-atmosphere interactions have played a role in late-season GrIS melt events spanning the end of boreal summer through autumn (e.g. Doyle et al., 2015; Stroeve et al., 2017). We posit that if Baffin Bay open water were to influence GrIS late-season melt events, the heat accumulated in the marine layer from ocean-to-atmosphere turbulent fluxes, would be transferred directly to the ice sheet by onshore westerly winds. In addressing this hypothesis, our analyses are geographically focused on the western slope of the GrIS with emphasis on the K-transect (**Fig. 1**) as this area – with its two on-ice AWS networks (described in Section 2.1) – is rich with in situ records relative to the remainder of the ice sheet. We analyze data from these in situ sources and additionally from a global atmospheric reanalysis and regional climate models to address potential links between GrIS late season melt and the local-scale Baffin Bay marine layer for the period of overlapping data, 2011–2015. For completeness, we subsequently expand the scale of meteorological analyses to consider the influence of greater northwest Atlantic synoptic patterns on the melt episodes. The paper is organized in the following manner: Section 2 outlines data sources, Section 3 describes methods employed, Section 4 covers the local and synoptic-scale atmospheric interactions with GrIS melt, Section 5 discusses key results, and Section 6 offers concluding remarks and makes suggestions for future research.

Deleted: meteorological

Deleted: and global meteorological re-analyses

Deleted: as follows

Deleted:

2 Data

2.1 Passive microwave records

Sea ice data are from the National Oceanic and Atmospheric Administration/National Snow and Ice Data Center (NSIDC) Climate Data Record of Passive Microwave SIC v3r1 product distributed by NSIDC (Meier et al., 2017). We use the "Goddard-merged" SICs that are produced using a combination of the NASA Team and Bootstrap algorithms applied to satellite passive microwave brightness temperatures (Peng et al., 2013). Daily observations are available over the 1979–2015 period at a 25 km by 25 km nominal grid spacing. The time series of daily SIC at each grid cell were used to identify the sea ice date of advance (DOA), which is the date when SIC increases to 15% for the first time following the sea ice extent (SIE) minima after Steele et al. (2019). Regional mean DOAs for Baffin Bay were obtained from Bliss et al. (2019). The local DOA was determined from the time series of SICs between 1 October and 31 March at each grid cell, then the local mean DOA was computed from 13 grid cells within the domain 66.5 to 67.5°N and 53 to 55°W. SIE was computed by summing the area of grid cells (in km^2) where SIC≥15%. At the same spatial resolution as the SIC product, the passive microwave daily GrIS melt time series of Mote (2007, 2014) is also used to classify the ice surface environment in a binary manner (i.e. melt/no melt). Following the Ohmura and Reeh (1991) topographic regions, we assess GrIS melt conditions on the west-central portion of the ice sheet bounding the K-transect.

Deleted:

Deleted: M

2.2 AWS data

Meteorological conditions from two AWS networks, the Programme for Monitoring of the Greenland Ice Sheet (PROMICE; stations prefix "KAN") and Utrecht University Institute for Marine and Atmospheric Research

(hereafter IMAU; stations prefix "S"), are used in this study (**Fig. 1**). To examine the possible Baffin Bay open water influence on observed surface air temperatures from the approximate terminus position nearest the ocean upslope across the longitudinal extent of the K-transect (referenced herein as the combination of PROMICE and IMAU stations), we conduct analyses based on temperature conditions monitored at KAN_B (see Section 3 for details). The operational record of KAN_B began in 2011 and represents the starting year for analysis, while the DOA record concludes in 2015 marking the end of our study period. Data are obtained and analyzed from seven weather stations distributed across the K-transect at ~67°N during this period. The transect spans an area from low-elevation tundra, approximately 1 km inland from the ice sheet glacier terminus (KAN_B), to the lower accumulation area (~1800 m) at >140 km from Russell Glacier terminus (KAN_U; see **Fig. 1** & **Table 1**). AWS data used here are recorded at approximately 2–3 m above the surface, though the heights of the air temperature sensors are known to fluctuate due to snow accumulation and melt season ablation (Charalampidis et al., 2015). Daily mean air temperature (°C), wind speed (ms^{-1}), and wind direction (0–360°) are obtained from IMAU and PROMICE station networks. The data series are mostly complete for the study period, and the few missing values are filtered out prior to analyses. Additional details on the respective PROMICE and IMAU AWS programs can be found in van As et al. (2011) and Smeets et al. (2018). We supplement K-transect data with daily mean DMI AWS surface air temperatures obtained from Sisimiut (WMO code 4234) and Kangerlussuaq (WMO code 4321). These data are used to further evaluate spatial links between local Baffin Bay open water and air temperatures from the tundra regions below the K-transect (Cappelen, 2018, 2019; **Fig. 1**).

Deleted: In order to include the westernmost PROMICE station

Deleted: that is situated approximately 1 km away from the ice-sheet margin, analyses

Deleted: i

Deleted: and

Deleted: with the end of the DOA record in 2015

Deleted: a height of

Deleted: at

Deleted: observed values

Deleted: Most d

Deleted: but

Deleted: or erroneously low

Deleted: in the temperature and wind variables

2.3 Atmospheric reanalysis and regional climate model fields

A number of ERA-Interim reanalysis (Dee et al., 2011) variables are analyzed at their native 80-km spatial resolution to assess atmospheric conditions across Greenland and the northwestern Atlantic Arctic sector. ERA-Interim surface and upper-air temperatures, wind speeds, and moisture conditions exhibit relatively small biases compared to Arctic observations (Bromwich et al., 2016). Regional climate models MAR and RACMO are also forced with ERA-Interim fields at their lateral boundaries. Tropospheric winds and specific humidity from the 1000 to 200 hPa (1000-200) atmospheric layer are used to calculate a moisture flux variable referred to as integrated water vapor transport (IVT); IVT is then classified using a self-organizing map (SOM) approach (see formal description in the Methods section below). Surface-atmosphere interactions and regional atmospheric circulation characteristics are further evaluated using ERA-Interim fields including mean sea-level pressure (MSLP), 10-meter (10-m) winds, latent and sensible heat fluxes, 500 hPa geopotential heights (GPH), and winds averaged over the 1000-700 hPa layer.

Deleted: are selected

Deleted: for the

Deleted: nalysis of

Deleted: 2

Deleted: -

Deleted: with

Deleted: data

Deleted: mean winds at the native 80 km resolution

Deleted: 2

Wind speed and direction at 10-m and 850 hPa from MAR and RACMO are evaluated to understand low-level atmospheric flow over ocean-land-ice sheet areas surrounding the K-transect. Secondarily, we briefly discuss inter-model differences within the planetary boundary layer and biases against AWS observations. Both regional climate models are specifically developed for simulating polar weather and climate, in particular over the Greenland ice sheet (e.g., Fettweis et al., 2011; Noël et al., 2018). MAR v3.9 fields at 15 km are used here (see Fettweis et al. 2017 for a detailed model description). Relative to MAR v3.8 used in Delhasse et al. (2018), the main changes to MAR v3.9 consist of enhanced computational efficiency, adjustments to some of the snow model parameters to better compare with in situ observations, and improved MAR dynamical stability by increasing the atmospheric filtering.

RACMO2.3p2 fields (hereafter referenced as RACMO2) at a horizontal resolution of 5.5 km are also used (Noël et al., 2018). Model physics have not changed relative to the previous 11 km version described in Noël et al. (2018). The refined spatial resolution of the host model improves the depiction of topographically complex terrain at the GrIS margins, such as small peripheral glaciers and ice caps, and the representation of near-surface, local winds.

2.4 North Atlantic atmospheric indices

Daily atmospheric indices are examined to characterize near-surface and upper-level conditions within a historical context. The Greenland Blocking Index (GBI) (Hanna et al., 2018) describes daily mean 500 hPa GPH values from 60-80°N and 20-80°W. The North Atlantic Oscillation (NAO) index used here is adapted from Cropper et al. (2015) and represents station-based daily MSLP differences between Iceland and the Azores. Both versions of the respective indices are normalized by their day of year means and standard deviations for the common 1951–2000 base period.

3 Methods

Above-freezing daily air temperatures at on-ice AWS locations represent an indicator of ice-sheet melt (Hock 2005). A composite approach is applied to characterize atmospheric conditions underlying late-season GrIS melt events, defined here as occurring at the conclusion of boreal summer (i.e. late August) and during autumn preceding sea ice advance on Baffin Bay (**Table S1**). Two constraints are placed on the composite analyses. The first constraint involves the length of the analysis period prior to DOA. Baffin Bay ice freeze onset dates and sea surface temperatures have shown a two month lead time and positive, significant correlation with west Greenland coastal air temperature variations (Hanna et al., 2009; Ballinger et al., 2018). Composites are constructed over a similar two-month (60-day) period with data additionally sub-divided into 60-31 day (i.e. [-60,-31]) and 30-1 day (i.e. [-30,-1]) bins preceding each Baffin Bay DOA from 2011 to 2015. Regarding the second constraint, the composite technique is intended to isolate meteorological processes most common during KAN_B daily mean air temperature events of ≥0°C (T+) versus <0°C (T-) and the spatial consistency of such conditions across the longitudinal extent of the transect. To resolve the spatial cohesiveness of melt events along the K-transect, daily mean air temperatures at each K-transect station are composited (i.e. averaged) for KAN_B T+ and T- days in the [-60,-31] and [-30,-1] periods. On average during 2011-2015, KAN_B T+ events characterize ~46% of days in the [-60,-31] period, while [-30,-1] events are less frequent and occur 9% of days preceding Baffin Bay DOA. T+ comparisons between KAN_B and other K-transect stations are provided in **Table 2**. Temporal overlap between above-freezing temperatures at KAN_B versus S5 (77%) and KAN_L (46%) in columns 2-3 of **Table 2** suggest spatial coherence in the physical mechanisms forcing melt at least across part of the lower ablation area.

In a similar fashion to Carr et al. (2017), a Wilcoxon test is used to evaluate differences in atmospheric variables and indices between T+ versus T- events. This nonparametric test is intended for continuous data series that do not follow underlying assumptions of the normal distribution making it appropriate for comparative analyses between extreme and non-extreme meteorological observations. The null hypothesis of no difference in atmospheric conditions between cases is rejected at the 95% confidence level when $p \leq 0.05$.

To classify synoptic patterns of atmospheric moisture transport about Greenland, integrated water vapor transport (IVT) is calculated from ERA-Interim data following Eq. (1):

Deleted: geopotential height

Deleted: mean sea-level pressure

Deleted: Through lead/lag correlations of recent data series of ≥30 years, Hanna et al. (2009) and Ballinger et al. (2018a) noted

Deleted: coverage

Deleted: in the preceding

Deleted: s

Deleted: to be

Deleted: ly and

Deleted: ly

Deleted: ed

Deleted: here

Deleted: A paucity of T+ events over the 30 days post-Baffin DOA limits analyses to the aforementioned periods before the development of extensive, seasonal sea ice coverage.

Deleted: Second

Formatted: Font: Bold

Deleted: conditions

Deleted: Following the methodology used in Mattingly et al. (2016, 2018), daily

Deleted: resolved

Deleted: by calculating IVT as in

$$\mathrm{IVT} = \frac{1}{g}\int_{1000\ \mathrm{hPa}}^{200\ \mathrm{hPa}} qV\ dp \quad (1)$$

where g is gravitational acceleration (9.80665 m s^{-2}), q is specific humidity (g kg^{-1}), V is the vector wind (m s^{-1}), and dp represents the difference between atmospheric pressure levels. Pressure levels are spaced at 50 hPa intervals between 1000 hPa and 500 hPa, and 100 hPa intervals from 500 hPa to 200 hPa. To control for the IVT seasonal cycle, the percentile rank of IVT (IVT PR) is calculated by comparing 6-hourly IVT values at each grid point to the distribution of all IVT values within a 31-day centered window at that grid point during 1980-2016. The four 6-hourly IVT PR values during each day are then averaged to generate daily mean IVT PR values.

Daily mean IVT PR data are classified using the SOM technique to produce a matrix of moisture transport patterns, or nodes, that typically occur over the Greenland region. The SOM is based on an unsupervised machine learning algorithm that classifies each daily IVT PR field into the closest matching SOM node. As in Mattingly et al. (2016), we utilize a 5x4 SOM configuration. We further classify SOM nodes—based on visual inspection of IVT PR patterns over Greenland—into "wet" (anomalously high IVT PR over Greenland), "neutral" (near climatological median IVT PR), and dry (anomalously low IVT PR) SOM node groups, and test whether the frequency of IVT patterns falling into each node group differs across T+ and T- events.

4 Results

4.1 Characteristics of Baffin Bay and west Greenland late-season melt

Time series depicting the conclusion of melt conditions across Baffin Bay and the western GrIS are shown in **Fig. 2**. Later sea ice formation is apparent in the DOA series, particularly from around 2000. Similarly, the start of the last ≥3-day sequence of Region 3 (west-central Greenland; see inset in **Fig. 1**) 2% or 4% melt area also suggests progressively later melt (and a later onset of freezing conditions). A significant break in the 2% series is highlighted by a drastic increase in variability from 1979–1999 (σ=21.17) to 2000–2015 (σ=44.25) that is also present in the annual discharge records from the nearby Watson River and Tasersiaq ice sheet catchments (Ahlstrøm et al., 2017; van As et al., 2018). Differences between the beginning of Baffin Bay sea ice advance and the end of the ice sheet melt season have clearly narrowed in part due to regional melt season lengthening. Some GrIS melt events since 2000 have notably occurred after seasonal sea ice formation (i.e. 2002, 2004–2005, 2010).

Relative to the climatology defined as 1981–2010, sea ice advanced ~11d earlier in 2011 and on average ~6d later in 2012–2015 (**Table S1**). Inspection of the DOA for individual grid cells adjacent to the Sisimiut AWS, which is labeled 4234 in **Fig. 1** and located ~150 km west of the K-transect ice sheet margin, reveals a northward-extending notch where ice forms ~30–60d later than the Baffin-wide DOA (**Fig 3**). Interannual differences in the region's ice cover advance, such as those observed 2011-2015, often depend on physical factors including regional winds, ocean heat transport, and water-mass changes (Myers et al., 2009; Ribergaard, 2014). For instance, strong offshore winds and poleward circulation of warm water from the West Greenland Slope Current often contribute to the local open water persistence, while southward Arctic Water transports support earlier ice formation patterns found in the east and north (Curry et al., 2014).

4.2 Local meteorology of melt versus non-melt cases

Composites of air temperature, wind speed and direction by KAN_B T+ and T- events are shown in **Fig. 4**. Across the transect, composite air temperature differences (T+ minus T- events) are warmer by roughly 7 to 8°C in

Deleted: T

Deleted: is then

Formatted: Indent: First line: 0.5"

Deleted: within a 30-day moving window is calculated to account for the seasonal cycle of IVT, and

Deleted: This study uses the same SOM dimensions, training parameters, and IVT composites a

Deleted: the same

Deleted: values

Deleted: as these authors

Deleted: Dates marking the

Deleted: end of the

Deleted: Northwest Atlantic melt season area

Deleted: **S1**

Deleted: Slow, upward change signifying l

Deleted: shown

Deleted: Meanwhile

Deleted: the

Deleted: e season

Deleted: (

Deleted: WMO code

Deleted:),

Deleted: ,

Deleted: **S**

Formatted: Not Highlight

Deleted: **2a-e**; **Fig S3**

Deleted: (WGSC)

Deleted: The spatial coherence of AWS observations across the K-transect along with inhomogenous GrIS Region 3 spatial melt patterns (e.g. southern GrIS pixels may pick up melt while those to the north do not experience the same conditions) and satellite pixel contamination issues at the tundra-ice interface, lead us to assess the melt events at the station level.

Deleted: **2**

Deleted: versus

the [-60,-31] window and 12 to 13°C in the [-30,-1] period (**Fig. 4a**). These differences tend to be smallest near the coast and increase to S6 in the mid-ablation area (~1000 m asl) where contemporaneous melt occurs ~14–16% of the time (**Table 2**).

KAN_B receives stronger, more southerly winds during T+ events that tend to become weaker and more southerly in autumn (i.e. [-30,-1]). There tends to be a general wind speed increase during T+ events, while direction remains more or less unaltered. Statistically significant directional change is more southerly, which is evident above the long-term equilibrium line altitude at S9. These katabatic winds are deflected to the right (southeasterly) by the Coriolis force as they travel toward Baffin Bay (van den Broeke et al., 2009) and may be aided additionally by synoptically-driven southerly winds. There is also evidence of wind speed intensification during [-60,-31] T+ events (~1–2 m s^{-1}) and to a lesser magnitude similar relationships hold during the [-30, -1] period (**Fig. 4b**). Increased wind speeds in T+ versus T- events are likely affected by the seaward enhancement of the pressure gradient aided by longer periods of nearshore open water (**Fig. 5**), while increased synoptic cyclone activity and lower MSLP over Baffin Bay during the summer-autumn season transition may also enhance offshore flows (McLeod and Mote, 2015). Wind speed increases may also initiate positive (downward) sensible heat fluxes associated with low elevation ice melt (**Fig. 6**). Just offshore, sensible and latent heat fluxes are generally negative (upward) in T- events and near zero to slightly positive during melt occurrences; positive turbulent flux differences in T+ versus T- events are apparent over oceanic areas from the Labrador Sea extending northward into Baffin Bay and the western edge of Greenland. This indicates decreased heat transfer from the ocean to atmosphere during T+ events relative to T- conditions, with southerly near-surface winds indicative of warm air advection (**Fig. 6**).

The K-transect offshore flows appear to represent a dynamic barrier to Baffin Bay marine layer intrusions. To further examine lower tropospheric flow across the ocean-land-ice interface, we similarly composite MAR and RACMO2 winds at 10-m and 850 hPa (**Figs. 7** and **8**). In general, the MAR and RACMO2 winds show directional consistency with overlaid PROMICE and IMAU winds with a slight southerly bias in both products for [-30,-1] at KAN_M and S9 in the upper ablation area. Simulated wind speeds are ~20-50% stronger during T+ versus T- events (not shown) as corroborated by most of the AWS observations (**Fig. 4b**), helping enhance sensible heat flux into the ice sheet in areas where near-surface temperatures are above freezing. T+ events in RACMO2 and MAR generally capture AWS observed wind speeds in the upper ablation area at KAN_M ($r^2 \geq 0.77$) and lower accumulation area at KAN_U ($r^2 \geq 0.77$) with low root mean squared errors (RMSE<1.50 m s^{-1} in all cases). A slight, positive bias in model-derived wind speed is evident at the ice sheet edge near KAN_B (MAR $r^2 = 0.33$, RACMO2 $r^2 = 0.58$). We note that height and therefore surface roughness differences between the AWS measurements (2–3 m) and regional model 10-m winds may explain a portion of the bias at KAN_B. The 10-m winds extending from the west Greenland tundra into eastern Baffin Bay are notably weak and northerly in T- events while T+ events are comparably stronger and southerly; **Figs. 7** and **8**).

4.3 The role of North Atlantic atmospheric patterns

Overplots of 500 hPa GPH, 1000-700 hPa mean wind, and IVT for Greenland and the surrounding northwest Atlantic region are shown in **Fig. 9**. Whereas T- events tend to be characterized by northerly winds over the 1000-700 hPa layer, the T+ events indicate southerly, on-ice transfer of subpolar air aided by the presence of an upper-level

Deleted: 2
Deleted: least
Deleted: Wind direction for T+ events are roughly southeasterly (<150°) in [-60,-31] and become more southerly (180°) in the [-30,-1] period (**Fig. 2c**) regardless of the wind speed (**Fig. 2b,d**). A
Deleted: ,
Deleted: [-60,-31] and KAN_U [-30,-1] winds are significantly more southerly during T+ events
Deleted: 2
Deleted: persistence
Deleted: S
Deleted: 4
Deleted: MSLP
Deleted: S5
Deleted: in
Deleted: with
Deleted: large,
Deleted: s
Deleted: in
Deleted: up to the WGSC
Deleted: s
Deleted: S5 and S6
Deleted: 3
Deleted: 4
Deleted: 2
Deleted: Except during [-30,-1] T+ events,
Deleted: t
Deleted: about the transect
Deleted: coast
Deleted: just offshore and
Deleted: calm and alongshore (i.e.
Deleted: in T+
Deleted: 3
Deleted: 4
Deleted: 5

trough over Baffin Island and downwind ridging over Greenland (see left versus right panel plots in **Fig. 9**, respectively). Higher GPH values are found over the ice sheet during T+ events as the 540 dam (i.e. 5400 m) contour extends across central Greenland, while the same contour is located south of the island in T- events. In both T+ cases, 1000-700 winds circulate poleward over the north Labrador Sea, aiding the heat and moisture transfer (as shown by heightened IVT values in T+ relative to T-) to the western Greenland ice sheet during [-60,-31] and [-30,-1] (**Fig. 9**). One notable difference between T+ cases is that low-level southerly winds originate deeper (~50°N) in the North Atlantic during the T+ [-30,-1] case. Local IVT maxima in both T+ events are concentrated over the southwest tip of the island, but remain ~100 kg m^{-1} s^{-1} near the K-transect. Comparatively, the depth integrated moisture flux over much of the west coast increases by a factor of 2–3 (4–5) during [-60,-31] ([-30,-1]) T+ versus T- events. This finding suggests that moist, onshore flow drives late season GrIS melt events, and moreover higher IVT is necessary to produce melt conditions as autumn progresses.

To further characterize and differentiate weather conditions by T± event, we utilize a SOM of IVT PR fields and composite SOM-classified daily IVT wet, dry, and neutral patterns (**Fig. 10a, b**). Analyses of the aggregated frequencies suggest that the wet patterns (with anomalously high IVT versus climatology) occur significantly more often in T+ versus T- events, and such nodes are more common by a factor of >4.5 in the [-30,-1] period. (**Fig. 10b**). While some caution should be exercised as the absolute frequency of these patterns decreases from roughly early ([-60,-31]) to late ([-30,-1]) autumn, humid atmospheric conditions appear to cause late-season melt. Increased incidence of wet patterns coincides with negative (positive) NAO (GBI) (both >|0.50| in T+ events; **Fig. 10c**), and a synoptic environment characterized by high surface (upper-level) pressure anomalies. This is confirmed by **Fig. 9**, whereby the higher 500 GPH values and 1000-700 mean winds during T+ events transport warm and moist air masses from Labrador Sea and southerly maritime latitudes to much of the western slope of the ice sheet to facilitate ablation-area melt.

5 Discussion

West Greenland summer and autumn air temperature variability and trends during the last 3–4 decades have shown strong response to increased frequency and intensity of Greenland high-pressure blocking, negative NAO patterns, and positive North Atlantic SST anomalies aided by background anthropogenic forcing (Hanna et al., 2016; McLeod and Mote, 2016; Ballinger et al., 2018a; Graeter et al., 2018). The current North Atlantic "warm period" since the mid-1990s is characterized by a positive Atlantic Multidecadal Oscillation phase and rising SSTs around southwestern Greenland (Myers et al., 2009; Ribergaard, 2014), including just offshore of Sisimiut (WMO code 4234 in **Fig. 1**) (orthogonal trend = +0.03°C $year^{-1}$, $p<0.05$, for 1995-2015 period using the SST product described in Ballinger et al., 2018b). Warming waters around the island are influencing Baffin Bay sea ice and west GrIS melt processes (Hanna et al., 2013; McLeod and Mote, 2015; Ballinger et al., 2018a) and seasonality toward earlier melt and later freeze (Stroeve et al., 2017). This melt area about K-transect suggests local low SIC and open water, inferred upward turbulent atmospheric heating, and onshore winds could influence nearby terrestrial melt events. Moreover, Sisimiut SSTs fluctuate with air temperatures (over the 60 days preceding DOA) in a statistically significant fashion for 2013-2015 at most K-transect stations with some distance decay noted upslope from the edge of the ablation area at S9 (**Fig. S1**). Summer and autumn west Greenland near-coastal air temperatures are modulated by the thermal

Deleted: 5
Deleted: Comparatively h
Deleted: with
Deleted: ,
Deleted: which tends to distinguish solid and liquid precipitation,
Deleted: ing
Deleted: in T+ events
Deleted: but
Deleted: areas
Deleted: of upward, turbulent heat flux (**Figs. S5** and **S6**),
Deleted: 5
Deleted: ,
Deleted: or higher
Deleted: signaling a concentration of
Deleted: and condensational processes over the ice sheet that
Deleted: the
Deleted: above-freezing air temperatures
Formatted: Font: Bold
Formatted: Font: Bold
Formatted: Font: Bold
Deleted: identified by Mattingly et al. (2016)
Deleted: 6
Deleted: a
Deleted: enhance
Deleted: 6
Deleted: b
Deleted: 5
Deleted: 6

properties of bordering SSTs (Hanna et al., 2009; Ballinger et al., 2018a). Interannual differences in the strength of SST-air temperature relationships (i.e. 2013–2015 versus 2011–2012) suggest: 1) processes driving warming ocean waters and air temperatures over the GrIS are independent when disparate wind directions occur at or near the ocean-tundra-ice sheet boundaries in years of weak-to-zero correlation (e.g. katabatic flows contrasting near-coastal barrier flows (van den Broeke and Gallée, 1996)), or alternatively 2) large-scale atmospheric circulation (i.e. near-surface and upper-level meridional winds) during years of positive, statistically significant correlations, modulates the near-shore surface open water and ice sheet air temperatures (Stroeve et al., 2017). We recognize that synoptic patterns may not necessarily be mutually exclusive in these examples, but the study objectives do not include comparison of high and low pressure features around Greenland for specific melt and non-melt events.

A number of studies have suggested that Baffin Bay marine layer interaction with the ice sheet boundary layer is obstructed by zonal and meridional flows such as the west coast plateau jet feature and katabatic winds (Hanna et al., 2009; Moore et al., 2013; Noël et al., 2014). Moore et al. (2013) noted a directionally consistent southerly 10-m wind field extending over the western half of Greenland in summer and winter, while observational studies similarly indicate a high frequency of southerly-to-southeasterly winds over the K-transect (van den Broeke et al., 2009). Southerly (easterly) 10-m winds are strongly linked to melt across two thirds (the southern third) of the ice sheet (Cullather and Nowicki, 2018). For an expanded spatial perspective, we briefly examine air temperatures at the next PROMICE station installment approximately 700 km north at Upernavik (UPE; 72.89°N). We find UPE_L (220 m asl on the ice sheet) melt occurs the day of KAN_B T+ events on >50% of occasions in both [-60,-31] and [-30,-1] windows (not shown). This suggests that above-freezing near-surface air often penetrates at least to PROMICE station UPE_L with a relatively warm air mass engulfing much of the west coast. Our observational and regional model analyses further show that homogenous low-level winds extend coastward at least to the tundra-ice sheet interface near KAN_B (see **Figs. 4**c, 7, and 8) and produce a "blocking effect" that inhibits the inland penetration of near-surface air from Baffin Bay (Noël et al., 2014). Of note, the katabatic mechanism becomes stronger as Baffin Bay DOA approaches in late autumn, with more pronounced radiational cooling over the ice sheet further supporting winds that prevent incursions of local marine air (van As et al., 2014).

If late season K-transect melt is minimally influenced by local Baffin Bay open water, then what physical mechanisms drive the melt events? Composites of the AWS K-transect observations and complementary regional model output indicate that recent late-season melt events tend to be driven by southerly synoptic patterns as opposed to local marine forcing. We provide evidence of this physical forcing by [-60,-31] and [-30,-1] T+ composites that show southerly flows of more warm, moist maritime air of lower latitude origins relative to T- cases. As shown in **Fig. 9**, during the former event period, air is transferred off northern Labrador Sea to the west coast, while a path of more southerly flow directs moist North Atlantic air masses onto Baffin Bay and southwestern Greenland in the period immediately preceding DOA. These "wet" synoptic patterns occur frequently under anomalous (>|1σ|) positive GBI and negative NAO values (**Fig. 10**b, c). We surmise from Mattingly et al. (2018) that such patterns are particularly moisture-rich (≥85th percentile IVT climatological values) and often accompanied by atmospheric rivers impacting Greenland, and their occurrence causes ablation area melt in non-summer, low insolation months through cloud radiative effects (i.e. increased downward longwave radiation transfer into the ice surface), condensational latent heat

Deleted: forcing
Deleted: ,
Deleted: manuscript
Deleted: 2
Deleted: 3
Deleted: 4
Deleted: 5
Deleted: 6
Deleted: a
Deleted: b

release, increased near-surface winds and turbulent heat flux, and liquid precipitation (Doyle et al., 2015; Binder et al., 2017; Oltmanns et al., 2019). The southerly winds that propagate moisture northward off the northwestern Atlantic Ocean are a product of amplified upper-level geopotential height patterns and meridional winds in T+ versus T- events extending from Denmark Strait and Irminger Sea on the east coast of Greenland onto the ice sheet (**Fig. 9**). Mid-tropospheric ridging, which is more pronounced in [-30,-1] than [-60,-31] events, supports southerly winds that funnel heat and moisture from likely deeper in the Atlantic basin to Baffin Bay and southwest Greenland to stimulate sea ice and GrIS ablation area melt conditions (Ahlstrøm et al., 2017; Ballinger et al., 2018a,b; Hanna et al., 2018). Cullather and Nowicki (2018) similarly find collocated, positive MSLP, and 500 hPa GPH anomalies over Denmark Strait and Irminger Sea tend to be associated with melt events in the basin encompassing the K-transect. Our analyses suggest that ocean-to-atmosphere turbulent fluxes are suppressed over Baffin Bay during T+ events, presumably due to the synoptic-scale warm air advection regime reducing the temperature and humidity gradients between the sea surface and atmosphere (Aemisegger and Papritz, 2018). Results further support North Atlantic-air-ice sheet coupling, rather than localized Baffin Bay ocean-atmosphere processes, as a strong driver of transition season melt before sea ice advances south of the K-transect. Synoptic patterns associated with negative summer NAO and positive GBI incidence strongly influence these melt events (**Fig. 10a, b, c**), prompting decreases in SMB, and increase in the K-transect equilibrium line altitude over the last 10-15 years (Hanna et al., 2013; Smeets et al., 2018).

6 Conclusions

Temporal co-variability between GrIS and Arctic sea ice mass loss suggests a possible feedback whereby adjacent open water conditions, ocean-to-atmosphere heat flux, and on-ice winds affect inland melt during the end of the melt season. Based on our 2011–2015 analyses bridging the end-of-summer/early autumn melt to the date of first-year Baffin Bay sea ice advance, we do not find evidence to support the hypothesis that local open water, resultant turbulent heating, and onshore winds have a pronounced impact on inland ice melt events. These thermodynamic processes, in particular, directly influence coastal air temperatures and have a fingerprint on marine outlet glacier behaviors (Carr et al., 2017), but are shown here to be inhibited by topographically-influenced flows and synoptic patterns whose interactions are not mutually exclusive. Furthermore, Baffin Bay warming coupled with a longer autumn open water period has been hypothesized to stimulate and invigorate upper-level, high-pressure blocking that promotes southerly air advection over the west Greenland coast (Ballinger et al., 2018a). This is consistent with the main conclusions of Noël et al. (2014), which suggest that while warming waters around Greenland minimally affect SMB beyond enhancing tidewater glacier retreat rates SST forcing may indirectly influence GrIS SMB changes through impacts on atmospheric circulation. However, in terms of direct forcing by the local marine layer, beyond a near-coastal influence, our AWS, regional, and synoptic wind analyses suggest that Baffin Bay does not represent a substantial advective heat and moisture source to the ice sheet during our 5-year analyses.

Future late season analyses, perhaps reconstructing K-transect meteorological conditions back to the origins of the modern sea ice record, might be insightful in comparing local ocean-ice sheet interactions spanning the 1990s shift from colder to warmer Baffin Bay summer SSTs (Ballinger et al., 2018a). Assessing the temperature and pressure gradients and their vertical profiles derived from retrospective analyses would also be useful to categorize the structure, magnitude, and direction of regional winds, including the katabatic regime, in attempting to provide a

Deleted: 5

Deleted: surface

Deleted: 6

Deleted: In

Deleted: no

longer-term perspective of analyses presented in this paper. Noël et al. (2014) hypothesized that future sea-surface warming may exacerbate the division between the local ocean and ice sheet by intensifying the temperature and pressure gradient and hence resulting katabatic winds. Baffin Bay climate and cryospheric changes in the last two decades suggest such an increased "blocking" mechanism may already be underway. Moreover, stronger katabatic winds might be enhanced further by an increasing intensity of autumn mid-troposphere high-pressure over Greenland (Hanna et al., 2018a, see their Fig. 1e). Synergistic future research should continue to monitor the spatial extent, drivers, and physical effects of late-season melt through observational products and regional modeling tools, including quantification of late season K-transect mass loss and runoff through the Watson River, contributions to subsurface/firn processes, and preconditioning effects on the following year's melt season.

Author Contributions. TJB and TLM conceived the study. TJB analyzed the observational data, with assistance from MP and SG, and led the writing of the manuscript. TLM developed and processed the satellite-derived GrIS melt data. KSM conducted the IVT classification and assisted with the creation of several figures. ACB developed the DOA series and contributed related figures. EH provided the daily GBI series, and DvA, CHR, PCJPS, MHR, and JC provided AWS or oceanographic data and support. BN and XF developed and processed regional model wind fields for RACMO2.3p2 and MAR v3.9, respectively. All authors provided valuable insights, feedback, and editing on manuscript drafts.

Acknowledgements. The KAN PROMICE weather stations are funded by the Greenland Analogue Project, and the IMAU K-transect stations are funded by the Netherland Institute for Scientific Research and its Netherlands Polar Programme. TJB acknowledges support from Texas State University, and IASC, NSF, and UAF for sponsoring and facilitating an APECS travel grant to attend the POLAR 2018 Open Science Conference where valuable project-related feedback was received. BN acknowledges funding from the Polar Program of the Netherlands Organization for Scientific Research (NWO) and the Netherlands Earth System Science Centre (NESSC). The authors thank David Bromwich and Jeffrey Miller for constructive comments on early results, and Thomas Cropper for making available his daily NAO series. Constructive remarks from Charalampos Charalampidis and two anonymous references were helpful in guiding manuscript improvements.

References

Aemisegger, F., Papritz, L.: A climatology of strong large-scale ocean evaporation events. Part I: Identification, global distribution, and associated climate conditions. J. Clim., 31, 7287-7312, doi:10.1175/JCLI-D-17-0591.1, 2018.

Ahlstrøm, A.P., Petersen, D., Langen P.L., Citterio, M., and Box, J.E.: Abrupt shift in the observed runoff from the southwestern Greenland ice sheet. Sci. Advan., 3, 1-7, doi:10.1126/sciadv.1701169, 2017.

Ballinger, T.J., Hanna, E., Hall, R.J. Miller, J., Ribergaard, M.H., and Høyer, J.L.: Greenland coastal air temperatures linked to Baffin Bay and Greenland Sea ice conditions during autumn through regional blocking patterns. Clim. Dyn., 50, 83-100, doi:10.1007/s00382-017-3583-3, 2018a.

Ballinger, T.J., Hanna, E., Hall, R.J., Miller, J., Ribergaard, M.H., Overland, J.E., and Høyer, J.L.: Anomalous blocking over Greenland preceded the 2013 extreme early melt of local sea ice. Ann. Glaciol., 59, 181-190, doi:10.1017/aog.2017.30, 2018b.

Bamber, J.L., Westaway, R.M., Marzeion, B. and Wouters, B.: The land ice contribution to sea level during the satellite era. Environ. Res. Lett. 13, 063008, doi:10.1088/1748-9326/aac2f0, 2018.

Binder, H., Boettcher, M., Grams, C.M., Joos, H., and Wernli, H.: Exceptional air mass transport and dynamical drivers of an extreme wintertime Arctic warm event. Geophys. Res. Lett., 44, 12028-12036, doi:10.1002/2017GL075841, 2017.

Bliss, A. C., Steele, M., Peng, G., Meier, W.N., and Dickinson, S.: Regional variability of Arctic sea ice seasonal change climate indicators from a passive microwave climate data record, Environ. Res. Lett., 14, 4, doi:10.1088/1748-9326/aafb84, 2019, .

Bromwich, D.H., Wilson, A.B., Bai, L.-S., Moore, G.W.K., and Bauer, P.: A comparison of the regional Arctic System Reanalysis and the global ERA-Interim Reanalysis for the Arctic. Q.J.R. Meteorol. Soc., 142, 644-658, doi:10.1002/qj.2527, 2016.

Cappelen, J.: Weather observations from Greenland 1958-2017. Observation data with description. DMI Report 18-08. Copenhagen, Denmark, 2018.

Cappelen, J.: Weather observations from Greenland 1958-2018. Observation data with description. DMI Report 19-08. Copenhagen, Denmark, 2019.

Carr, J.R., Stokes, C.R., and Vieli, A.S.: Threefold increase in marine-terminating outlet glacier retreat rates across the Atlantic Arctic: 1992-2010. Ann. Glaciol., 58, 72-91, doi:10.1017/aog.2017.3, 2017.

Charalampidis, C., van As, D., Box, J. E., van den Broeke, M. R., Colgan, W. T., Doyle, S. H., Hubbard, A. L., MacFerrin, M., Machguth, H., and Smeets, C. J. P. P.: Changing surface–atmosphere energy exchange and refreezing capacity of the lower accumulation area, West Greenland, Cryosphere, 9, 2163-2181, doi:10.5194/tc-9-2163, 2015.

Cropper, T., Hanna, E. Valente, M.A., and Jónsson, T.: A daily Azores-Iceland North Atlantic Oscillation index back to 1850. Geosci. Data J., 2, 12-24, doi:10.1002/gdj3.23, 2015.

Cullather, R.I., and Nowicki, S.M.J.: Greenland ice sheet surface melt and its relation to daily atmospheric conditions. J. Clim., 31, 1897-1919, doi:10.1175/JCLI-D-17-0447.1, 2018.

Deleted: , in preparation

Deleted: The

Curry, B. Lee, C.M., Petrie, B., Moritz, R.E., and Kwok, R.: Multiyear volume, liquid freshwater, and sea ice transports through Davis Strait, 2004-2010. J. Phys. Oceanog., 44, 1244-1266, doi:10.1175/JPO-D-13-0177.1, 2014.

Dee, D.P., Uppala, S.M., Simmons, A.J., Berrisford, P., Poli, P., Kobayashi, S., Andrae, U., Balmaseda, M.A., Balsamo, G., Bauer, P., Bechtold, P., Beljaars, A.C.M., van de Berg, L., Bidlot, J., Bormann, N., Delsol, C., Dragani, R., Fuentes, M., Geer, A.J., Haimberger, L., Healy, S.B., Hersbach, H., Hólm, E.V., Isaksen, L., Kållberg, P., Köhler, M., Matricardi, M., McNally, A.P., Monge-Sanz, B.M., Morcrette, J.-J., Park, B.K., Peubey, C., de Rosnay, P., Tavolato, C., Thépaut, J.-N., Vitart, F.: The ERA-Interim reanalysis: configuration and performance of the data assimilation system. Q. J. R. Meteorol. Soc., 137, 553–597, doi:10.1002/qj.828, 2011.

Delhasse, A., Fettweis, X., Kittel, C., Amory, C., and Agosta, C.: Brief communication: Impact of the recent atmospheric circulation change in summer on the future surface mass balance of the Greenland Ice Sheet, Cryosphere, 12, 3409-3418, doi:10.5194/tc-2018-65, 2018.

Doyle, S., Hubbard, A., van de Wal, R.S., Box, J., van As, D., Scharrer, K., Meierbachtol, T.W., Smeets, P.C.J.P., Harper, J.T., Johansson, E., Mottram, R.H., Mikkelsen, A.B., Wilhelms, F., Patton, H., Christoffersen, P., Hubbard, B.: Amplified melt and flow of the Greenland ice sheet driven by late-summer cyclonic rainfall. Nat. Geosci. 8, 647-653, doi:10.1038/ngeo2482, 2015.

Fettweis, X., Tedesco, M., van den Broeke, M., and Ettema, J.: Melting trends over the Greenland ice sheet (1958–2009) from spaceborne microwave data and regional climate models, Cryosphere, 5, 359-375, doi:10.5194/tc-5-359, 2011.

Fettweis, X., Box, J. E., Agosta, C., Amory, C., Kittel, C., Lang, C., van As, D., Machguth, H., and Gallée, H.: Reconstructions of the 1900–2015 Greenland ice sheet surface mass balance using the regional climate MAR model, Cryosphere, 11, 1015-1033, doi:10.5194/tc-11-1015, 2017.

Graeter, K.A., Osterberg, E.C., Ferris, D.G., Hawley, R.L., Marshall, H.P., Lewis, G., Meehan, T., McCarthy, F., Overly, T., and Birkel, S.D.: Ice core records of west Greenland melt and climate forcing. Geophys. Res. Lett., 45, 3164-3172, doi:10.1002/2017GL076641, 2018.

Graham, R.M., Cohen, L., Petty, A.A., Boisvert, L.N., Rinke, A., Hudson, S.R., Nicolaus, M., and Granskog, M.A.: Increasing frequency and duration of Arctic winter warming events. Geophys. Res. Lett., 44, 6974-6983, doi:10.1002/2017GL073395, 2017.

Hanna, E. Cappelen, J., Fettweis, X., Huybrechts, P., Luckman, A., and Ribergaard, M.H.: Hydrologic response of the Greenland ice sheet: the role of oceanographic warming. Hydrol. Proc., 23, 7-30, doi:10.1002/hyp.7090, 2009.

Hanna, E., Mernild, S.H., Cappelen, J., and Steffen, K.: Recent warming in Greenland in a long-term instrumental (1881-2012) climatic context: I. Evaluation of surface air temperature records. Environ. Res. Lett., 7, 1-15, doi:10.1088/1748-9326/7/4/045404, 2012.

Hanna, E., Jones, J.M., Cappelen, J., Mernild, S.H., Wood, L., Steffen, K., and Huybrechts, P.: The influence of North Atlantic atmospheric and oceanic forcing effects on 1900-2010 Greenland summer climate and ice melt/runoff. Int. J. Climatol., 33, 862-880, doi:10.1002/joc.3475, 2013.

Hanna, E., Fettweis, X., Mernild, S.H., Cappelen, J., Ribergaard, M.H., Shuman, C.A., Steffen, K., Wood, L., and Mote, T.L.: Atmospheric and oceanic climate forcing of the exception Greenland ice sheet surface melt in summer 2012. Int. J. Climatol., 34, 1022-1037, 2014.

Hanna, E., Cropper, T.E., Hall, R.J., and Cappelen, J.: Greenland Blocking Index 1851–2015: a regional climate change signal. Int. J. Climatol., 36, 4847-4861, doi:10.1002/joc.4673, 2016.

Hanna E., Hall, R.J., Cropper, T.E., Ballinger, T.J., Wake, L., Mote, T., and Cappelen, J.: Greenland Blocking Index daily series 1851-2015: analysis of changes in extremes and links with North Atlantic and UK climate variability and change. Int. J. Climatol., 38, 3546-3564, doi:10.1002/joc.5516, 2018a.

Hanna, E., Fettweis, X., and Hall, R.J.: Brief communication: Recent changes in summer Greenland blocking captured by none of the CMIP5 models. Cryosphere, 12, 3287-3292, doi:10.5194/tc-12-3287, 2018b.

Hock, R.: Glacier melt: a review of processes and their modelling. Prog. Phys. Geog., 29, 362-391, doi:10.1191/0309133305pp453ra, 2005.

Holland, D.M., Thomas, R.H., de Young, B., Ribergaard, M.H., and Lybert, B.: Acceleration of Jakobshavn Isbrae triggered by warm subsurface ocean waters. Nat. Geoscience, 1, 659-664, doi:10.1038/ngeo316, 2008.

Markus, T., Stroeve, J. C., and Miller, J.: Recent changes in Arctic sea ice melt onset, freeze-up, and melt season length. J. Geophys. Res., 114, C12024, doi:10.1029/2009JC005436, 2009.

Mattingly, K.S., Ramseyer, C.A., Rosen, J.J., Mote, T.L., and Muthyala, R.: Increasing water vapor transport to Greenland Ice Sheet revealed using self-organizing maps. Geophys. Res. Lett., 43, 9250-9258, doi:10.1002/2016GL070424, 2016.

Mattingly, K.S., Mote, T.L., and Fettweis, X.L.: Atmospheric river impacts on Greenland ice sheet surface mass balance. J. Geophys. Res. Atmos., 123, 8538-8560, doi:10.1029/2018JD028714, 2018.

McLeod, J.T., and Mote, T.L.: Assessing the role of precursor cyclones on the formation of extreme Greenland blocking episodes and their impact on summer melting across the Greenland ice sheet. J. Geophys. Res., 120, 12357-12377, doi:10.1002/2015JD023945, 2015.

McLeod, J.T., and Mote, T.L.: Linking interannual variability in extreme Greenland blocking episodes to the recent increase in summer melting across the Greenland ice sheet. Int. J. Climatol., 36, 1484-1499, doi:10.1002/joc.4440, 2016.

Meier, W., Fetterer, F., Savoie, M., Mallory, S., Duerr, R., and Stroeve, J.: NOAA/NSIDC Climate Data Record of Passive Microwave Sea Ice Concentration, Version 3, Revision 1, National Snow & Ice Data Center, Boulder, Colorado (Accessed 18 December 2017), doi:http://dx.doi.org/10.7265/N59P2ZTG, 2017.

Mernild, S.H., Hanna, E., Yde, J.C., Cappelen, J., and Malmros, J.K.: Coastal Greenland air temperature extremes and trends 1890-2010: annual and monthly analysis. Int. J. Climatol., 34, 1472-1487, doi:10.1002/joc.3777, 2014.

Moore, G.W.K., Renfrew, I.A., and Cassano, J.J.: Greenland plateau jets. Tellus A, 65, 1748, 1-16, doi:10.3402/tellusa.v65i0.17468, 2013.

Moore, G.W.K.: The December 2015 North Pole Warming Event and increasing occurrence of such events. Sci. Rep., 6, 39084, doi:10.1038/srep39084, 2016.

Mote, T.L.: Greenland surface melt trends 1979-2007: Evidence of a large increase in 2007. Geophys. Res. Lett., 34, L22507, doi:10.1029/2007GL0311976, 2007.

Mote, T. L.: MEaSUREs Greenland Surface Melt Daily 25km EASE-Grid 2.0, Version 1. Boulder, Colorado USA. NASA National Snow and Ice Data Center Distributed Active Archive Center. doi:10.5067/MEASURES/CRYOSPHERE/nsidc-0533.001. Accessed 1 September 2017, 2014.

Myers, P.G., Donnelly, C., and Ribergaard, M.H.: Structure and variability of the west Greenland Current in summer derived from 6 repeat standard sections. Prog. Ocean., 80, 93-112, doi:10.1016/j.pocean.2008.12.003, 2009.

Noël, B., Fettweis, X., van de Berg, W.J., van den Broeke, M.R., and Erpicum, M.: Sensitivity of Greenland Ice Sheet surface mass balance to perturbations in sea surface temperature and sea ice cover: a study with the regional climate model MAR. Cryosphere, 8, 1871-1883, doi:10.5194/tc-8-1871, 2014.

Noël, B., van de Berg, W.J., van Wessem, J.M., van Mejgaard, E., van As, D., Lenaerts, J.T.M., Lhermitte, S., Munneke, P.K., Smeets, C.J.P., van Ulft, L.H., van de Wal, R.S.W., and van den Broeke, M.R.: Modelling the climate and surface mass balance of the polar ice sheets using RACMO2 – Part 1: Greenland (1958 – 2016). Cryosphere, 12, 811-831, doi:10.5194/tc-12-811, 2018.

Ohmura, A., and Reeh, N.: New precipitation and accumulation maps for Greenland. J. Glaciol., 37, 140-148, 1991.

Oltmanns, M., Straneo, F., and Tedesco, M.: Increased Greenland melt triggered by large-scale, year-round cyclonic moisture intrusions. Cryosphere, 13, 815-825, doi:10.5194/tc-13-815, 2019.

Onarheim, I.H., Eldevik, T., Smedsrud, L.H., and Stroeve, J.C.: Seasonal and regional manifestation of Arctic sea ice loss. J. Clim., 31, 4917-4932, doi:10.1175/JCLI-D-17-0427.1, 2018.

Overland, J.E., and Wang, M.: Recent extreme Arctic temperatures are due to a split polar vortex. J. Clim., 29, 5609-5616, 2016.

Peng, G., Meier, W.N., Scott, D.J., and Savoie, M.H: A long-term and reproducible passive microwave sea ice concentration data record for climate studies and monitoring, Earth Syst. Sci. Data, 5, 311–318, doi:10.5194/essd-5-311-2013, 2013.

Rennermalm, A.K., Smith, L.C., Stroeve, J.C., and Chu, V.W.: Does sea ice influence Greenland ice sheet surface-melt. Environ. Res. Lett., 4, 1-6, doi:107282/T36D5RDG, 2009.

Ribergaard, M.H.: Oceanographic investigations off west Greenland 2013. NAFO Scientific Council Documents, 14/001, 2014.

Serreze, M.C., and Stroeve, J.: Arctic sea ice trends, variability and implications for seasonal forecasting. Phil. Trans. R. Soc. A 373: 20140159, 2015.

Smeets, P.C.J.P., Kuipers Munneke, P., van As, D., van den Broeke, M.R., Boot, W., Oerlemans, H., Snellen, H., Reijmer, C.H., and van de Wal, R.S.W: The K-transect in west Greenland: Automatic weather station data (1993-2016). Arc., Antarc., and Alp. Res., 50, S100002, doi:10.1080/15230430.2017.1420954, 2018.

Steele, M., Bliss, A.C., Peng, G., Meier, W.N, and Dickinson, S.: Arctic sea ice seasonal change and melt/freeze climate indictors from satellite data, Version 1, National Snow & Ice Data Center Distributed Active Archive Center, Boulder, Colorado, doi:10.5067/KINANQKEZI4T, 2019.

Straneo, F., and Heimbach, P.: North Atlantic warming and the retreat of Greenland's outlet glaciers. Nature, 504, 36-43, doi:10.1038/nature12854, 2013.

Stroeve, J.C., Mioduszewski, J.R., Rennermalm, A, Boisvert, L.N., Tedesco, M., and Robinson, D.: Investigating the local-scale influence of sea ice Greenland surface melt. Cryosphere, 11, 2363-2381, doi:10.5194/tc-11-2363, 2017.

Stroeve, J.C., Schroder, D., Tsamados, M., and Feltham, D.: Warm winter, thin ice? Cryosphere, 12, 1791-1809, doi:10.5194/tc-12-1791, 2018.

van As, D., Fausto, R.S., and PROMICE Project Team: Programme for Monitoring of the Greenland Ice Sheet (PROMICE): first temperature and ablation records. Geol. Surv. Denmark Greenland Bull., 23, 73-76, 2011.

van As, D., Fausto, R.S., Steffen, K., and PROMICE project team: Katabatic winds and piteraq storms: observations from the Greenland ice sheet. Geol. Surv. Denmark Greenland Bull., 31, 83-86, 2014.

van As, D., Hasholt, B., Ahlstrøm, A.P., Box, J.E., Cappelen, J., Colgan, W., Fausto, R.S., Mernild, S.H., Mikkelsen, A.B., Noël, B.P.Y., Petersen, D., and van den Broeke, M.R., 2018: Reconstructing Greenland Ice Sheet meltwater discharge through the Watson River (1949-2017). Arc., Antarc., and Alp. Res., 50, S100010, doi:10.1080/15230430.2018.1433799, 2018.

van de Wal, R.S.W., Smeets, C.J.P.P., Boot, W., Stoffelen, M., van Kampen, R., Doyle, S.H., Wilhelms, F., van den Broeke, M.R., Reijmer, C.H., Oerlemans, J., and Hubbard, A.: Self-regulation of ice flow varies across the ablation area in south-west Greenland, Cryosphere, 9, 603-611, doi:10.5194/tc-9-603, 2015.

van den Broeke, M.R., and Gallée, H.: Observation and simulation of barrier winds at the western margin of the Greenland ice sheet. Q.J.R. Meteorol. Soc., 122, 1365-1383, 1996.

van den Broeke, M., Smeets, P., Ettema, J.: Surface layer climate and turbulent exchange in the ablation zone of the west Greenland ice sheet. Int. J. Climatol., 29, 2309-2323, doi:10.1002/joc.1815., 2009.

van den Broeke, M.R., Enderlin, E.M., Howat, I.M., Kuipers Munneke, P., Noël, B.P.Y., van de Berg, W.J., van Meijgaard, E., and Wouters, B.: On the recent contribution of the Greenland ice sheet to sea level change. Cryosphere, 10, 1933-1946, doi:10.5194/tc-10-1933, 2016.

van den Broeke, M., Box, J., Fettweis, X., Hanna, E., Noël, B., Tedesco, M., van As, D., van de Berg, W.J., van Kampenhout, L.: Greenland ice sheet surface mass loss: Recent developments in observation and modeling. Curr. Clim. Change Rep., 3, 345-356, doi:10.1007/s40641-017-0084-8, 2017.

Tables

AWS Station	Network	Latitude (°N)	Longitude (°W)	Elevation (m asl)	Distance to/from terminus (km)
KAN_B	PROMICE	67.13	50.18	350	1
S5	IMAU	67.08	50.10	500	6
KAN_L	PROMICE	67.10	49.95	670	12
S6	IMAU	67.07	49.38	1000	37
KAN_M	PROMICE	67.07	48.84	1270	61
S9	IMAU	67.05	48.22	1500	88
KAN_U	PROMICE	67.00	47.03	1840	142

Table 1. Summary details of the PROMICE and IMAU AWS stations utilized in this study, including their approximate geographic position (in decimal degrees), elevation, and distance from the ice sheet terminus moving west to east. KAN_B is located on the tundra, roughly 1 km to the west of the terminus. Distances are rounded to the nearest km as on-ice AWS sites are known to move ~50 - 150 m year^{-1} (van de Wal et al., 2015).

Deleted: east

AWS T Compare	T+ n[-60,-31]	T+ %[-60,-31]	T+ n[-30,-1]	T+ %[-30,-1]	T+ %[-60,-1]
S5 vs KAN_B	53	77	9	69	76
KAN_L vs KAN_B	32	46	8	62	49
S6 vs KAN_B	10	14	3	23	16
KAN_M vs KAN_B	2	3	1	8	4
S9 vs KAN_B	1	1	0	-	1
KAN_U vs KAN_B	0	-	0	-	-
∑ KAN_B T+ events	69	-	13	-	-

Table 2. Counts of above-freezing daily mean air temperature (T+) events (n), 2011-2015, and the percentage of contemporaneous overlap (%) between T+ events at KAN_B and S5, KAN_L, S6, KAN_M, S9, or KAN_U. The [-60,-31] and [-30,-1] periods reference time windows before respective annual dates of Baffin Bay sea ice advance (DOA). As an example, 77% of the time in the 30 to 60-day (i.e. [-60,-31]) window preceding Baffin DOA the T+ air temperature threshold at KAN_B is also observed at S5.

Figures

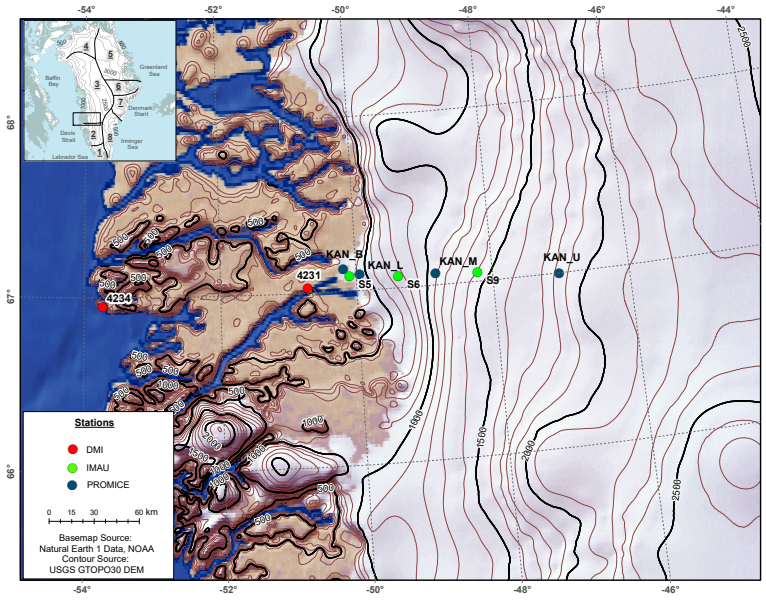

Figure 1. Study area map with PROMICE and IMAU K-transect sites and adjacent terrestrial DMI stations (Kangerlussuaq (WMO code 4231) and Sisimiut (WMO code 4234)). The inset displays the northwest Atlantic Arctic region with superimposed GrIS topographically-defined boundaries (adopted from Ohmura and Reeh (1991)).

Deleted: ,

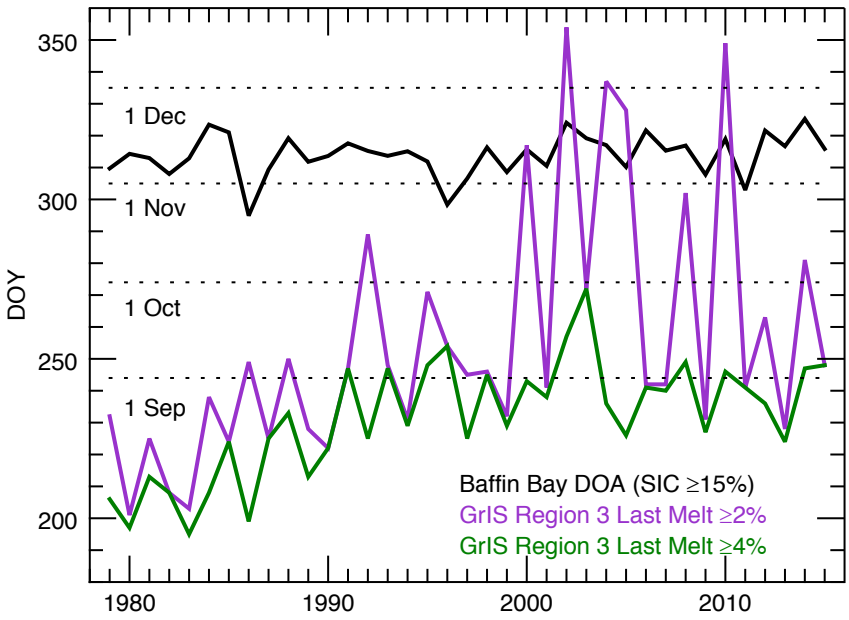

Figure 2. Passive microwave-derived time series, 1979-2015, of the Baffin Bay sea ice date of advance (DOA) and the date marking the beginning of the last 3-day period of at least 2% and 4% melt over Region 3 (see inset in **Fig. 1**) of the Greenland Ice Sheet (GrIS).

770

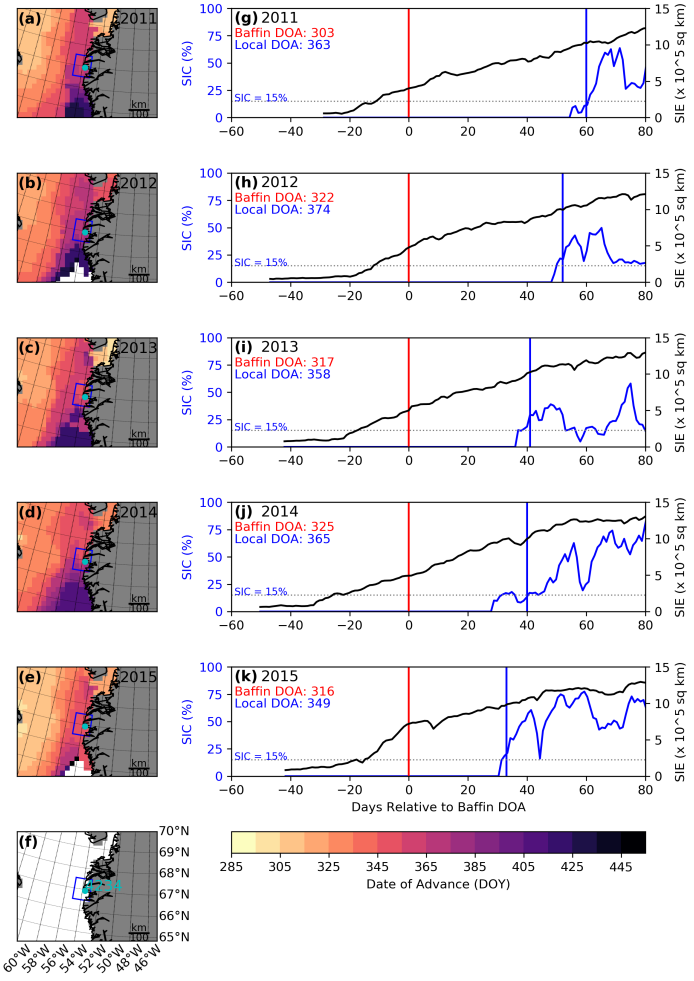

Figure 3. Maps of the Baffin Bay date of sea ice advance (DOA) for a-e) 2011-2015. The location of Sisimiut (WMO code 4234) is marked in cyan, white indicates locations where DOA was not observed and grey indicates land. Panel f) shows reference grid coordinates for maps a-e. DOY after 365 (or 366 in 2012) indicates that DOA occurs after 1 January the following year. Time series of sea ice extent (SIE) for the Baffin Bay region (black) and mean sea ice concentration (SIC) for the local domain (blue), 66.5 to 67.5°N and 53 to 55°W (blue polygon shown in a-f), relative to the Baffin-wide DOA (vertical red line) for g-k) 2011-2015. The vertical blue line shows the mean DOA for the local domain. The horizontal dotted line represents the 15% SIC threshold used to identify the DOA.

Formatted: Justified, Line spacing: 1.5 lines

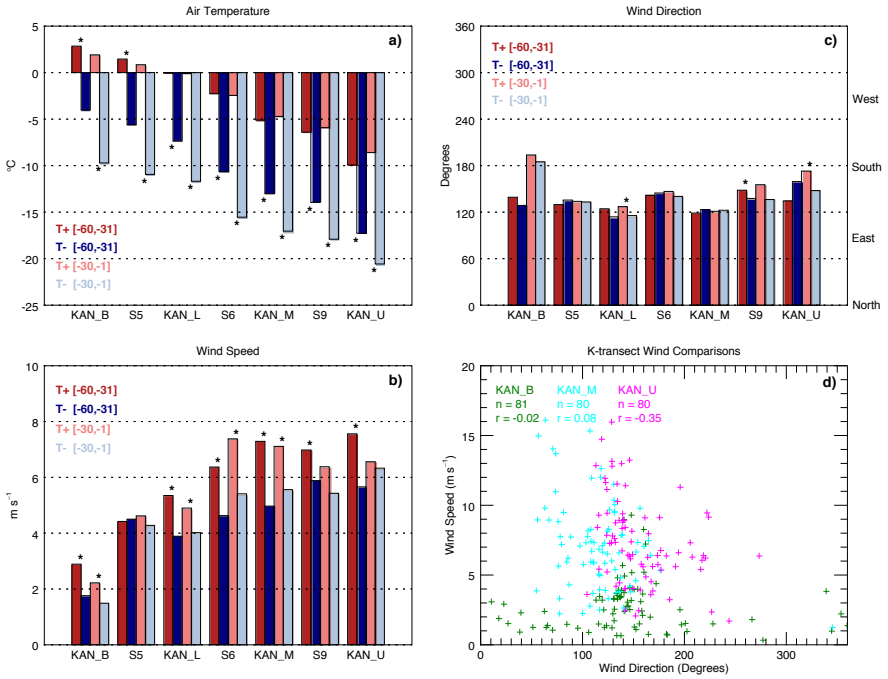

780

Figure 4. Composites of a) near-surface air temperature, b) wind speed, and c) wind direction for the T+ and T- events at KAN_B preceding the Baffin Bay date of sea ice advance (DOA), 2011-2015. Significant differences ($p \leq 0.05$) between T+ and T- composites over similar time windows are shown by an asterisk (*) between the bars. Panel d) shows daily mean wind speed as a function of direction for select, roughly equidistant K-transect PROMICE stations.

785

Deleted: 2

Deleted: s

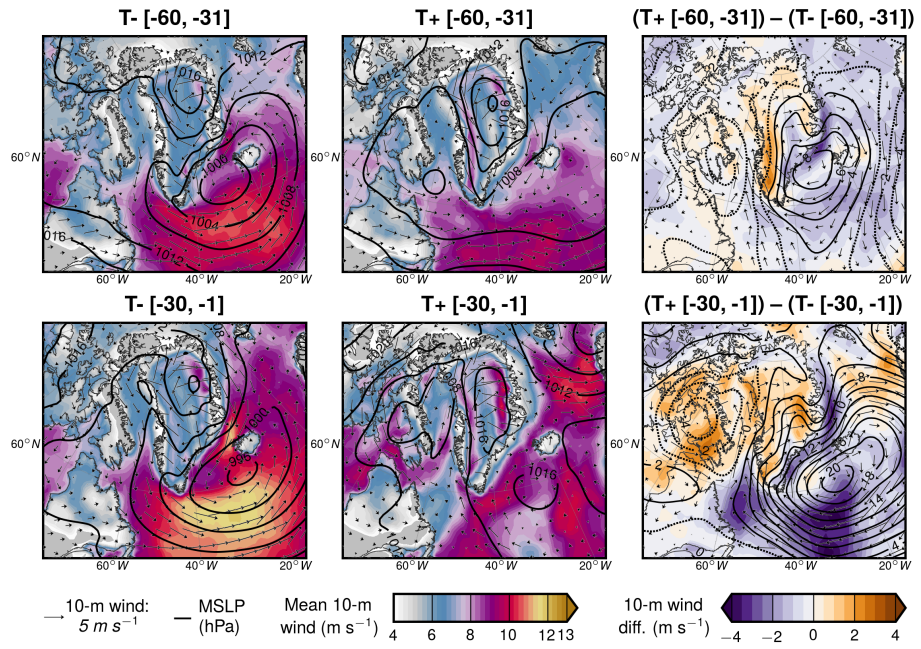

Figure 5. North Atlantic mean sea-level pressure (MSLP) and 10-m wind composites from ERA-Interim for T+ and T- events at KAN_B and their differences for the two periods preceding the Baffin Bay date of sea ice advance (DOA).

Formatted: Justified

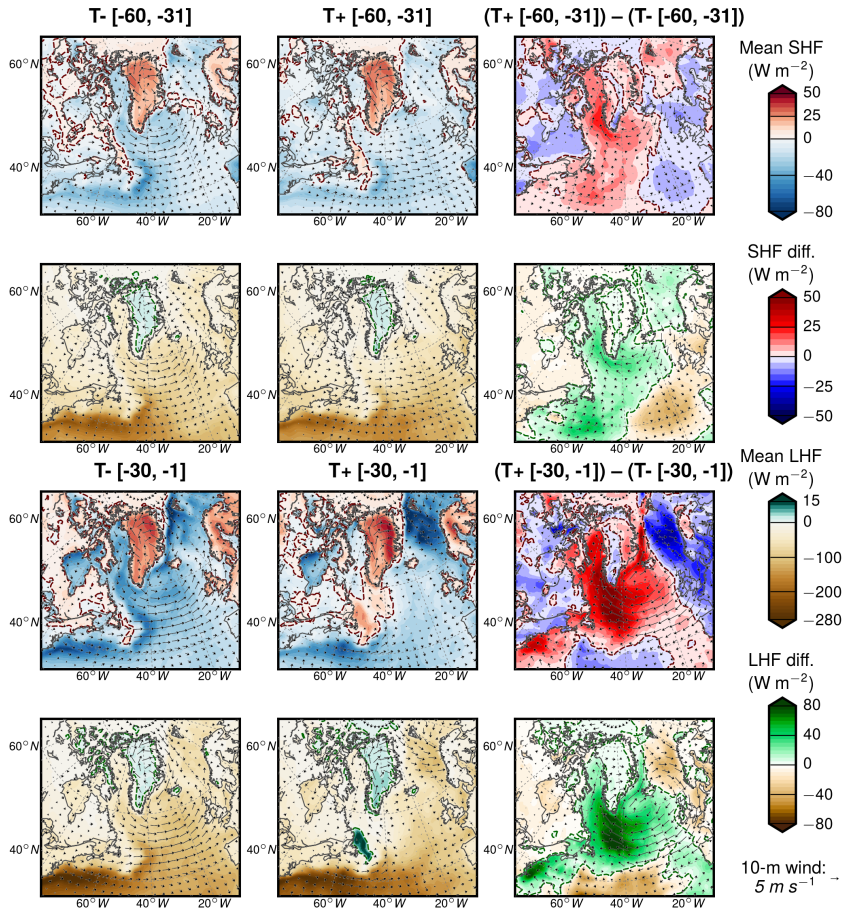

Figure 6. North Atlantic sensible heat flux (SHF), latent heat flux (LHF), and 10-m wind composites from ERA-Interim for T+ and T- events at KAN_B and their differences for the two periods preceding the Baffin Bay date of sea ice advance (DOA).

Formatted: Justified, Line spacing: 1.5 lines

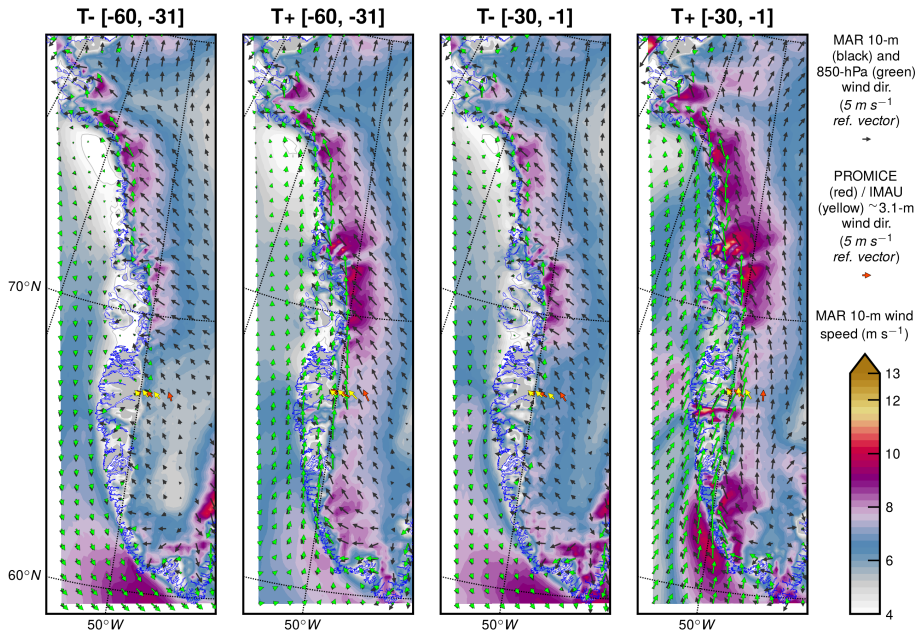

800 **Figure 7.** Composites of MAR 10-m (black arrows) and 850 hPa (green arrows) vector winds for the T+ and T- events at KAN_B preceding the Baffin Bay date of sea ice advance (DOA), 2011-2015. Wind observations from PROMICE (red) and IMAU (yellow arrows) are overlaid for reference.

Deleted: 3

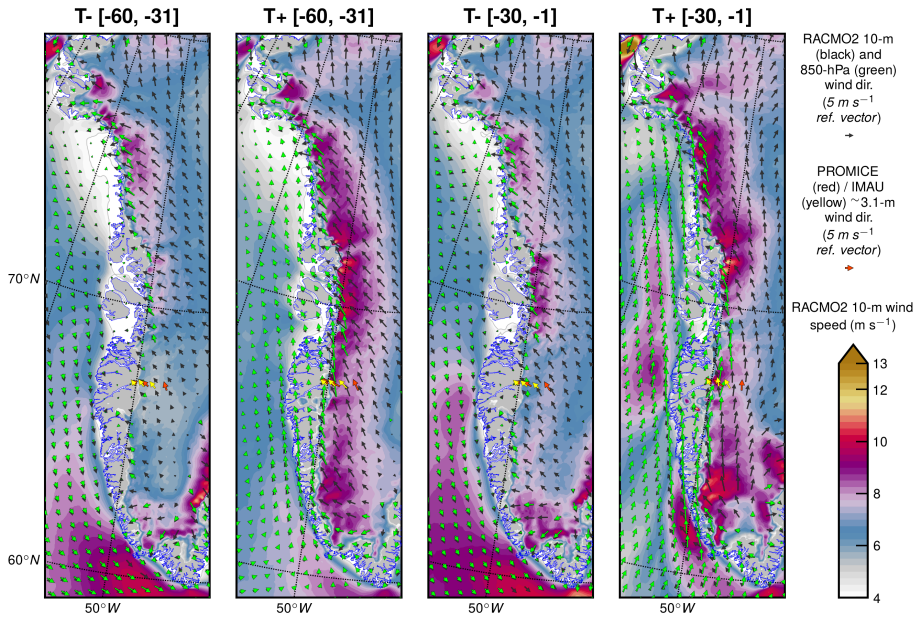

805

Figure 8. Composites of RACMO2 10-m (black arrows) and 850 hPa (green arrows) vector winds for the T+ and T- events at KAN_B preceding the Baffin Bay date of sea ice advance (DOA), 2011-2015 (refer to methods for details). Wind observations from PROMICE (red arrows) and IMAU (yellow arrows) are overlaid for reference.

Deleted: 4

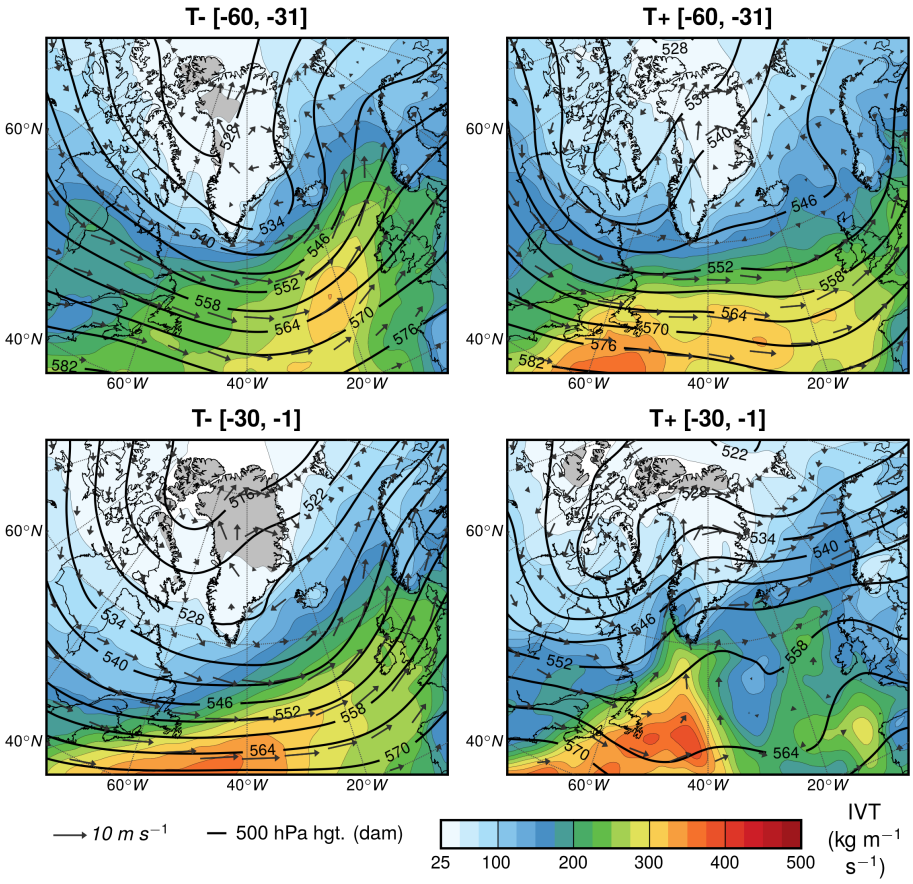

Figure 9. Composite plots of integrated vapor transport (IVT), 1000-700 hPa winds, and 500 hPa GPH from ERA-Interim for T+ and T- events at KAN_B for the two periods preceding the Baffin Bay date of sea ice advance (DOA).

Deleted: 5

Deleted: data

Deleted: ¶
¶

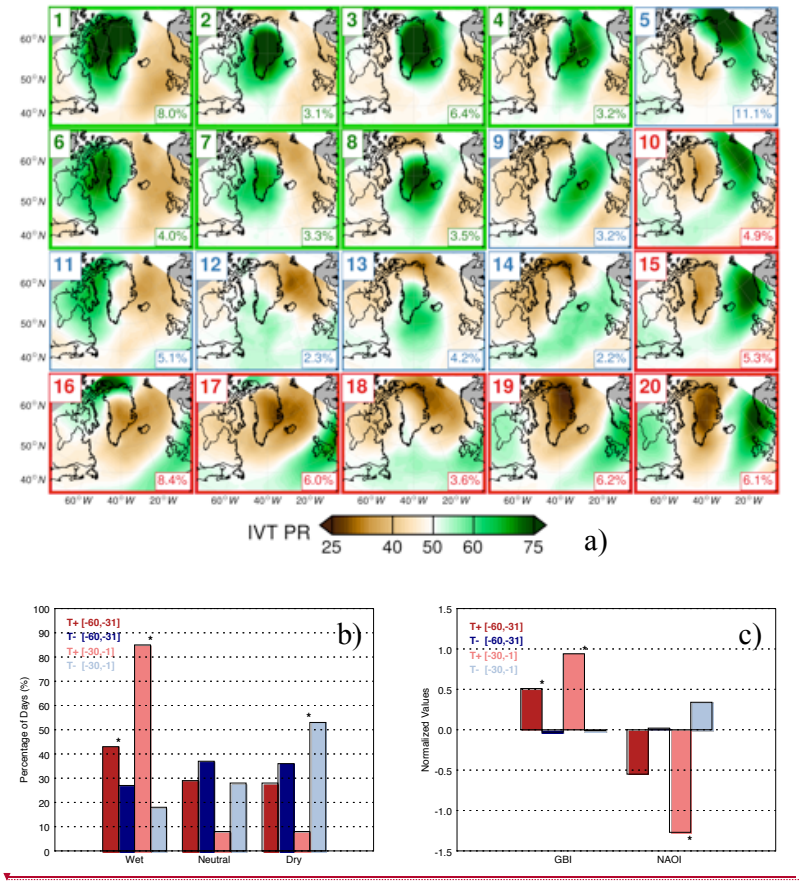

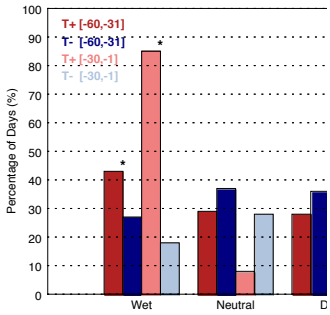

Deleted:

820 **Figure 10.** Percentile rank of integrated vapor transport fields (IVT PR) from ERA-Interim classified using a self-organizing map (SOM) approach a) and composites of b) IVT PR SOM node frequencies by wet, neutral and dry types (%). SOM aggregates in panel b) represent the ratio of each pattern's occurrence to the sum of all patterns for each time period and similarly colored bars sum to 100%. Composites presented in panel c) represent normalized Greenland Blocking Index (GBI) and North Atlantic Oscillation (NAO) values (unitless) for T+ and T- events at 825 KAN_B for the two periods preceding the Baffin Bay date of sea ice advance (DOA). Significant differences ($p \leq 0.05$) between T+ and T- composites over similar time windows are shown by an asterisk (*) between the bars.

Deleted: 6
Deleted: C
Deleted: a
Deleted: self-organizing map (
Deleted:)
Deleted: s
Deleted: and
Deleted: b
Deleted: SOM aggregates represent the ratio of each pattern's occurrence to the sum of all patterns for each time period and similarly colored bars sum to 100%.
Deleted: s